Estimation of velocity change using repeating earthquakes with different locations and focal mechanisms

Chinaemerem O. Kanu and Roel Snieder
Center for Wave Phenomena, Colorado School of Mines, Golden CO 80401

ABSTRACT
Codas of repeating earthquakes carry information about the time-varying properties of the subsurface or reservoirs. Some of the changes within a reservoir change the seismic velocity and thereby the seismic signals that travel through the reservoir. In characterizing these velocity changes, seismic signals are often influenced by changes in other properties of the reservoir such as fluid migration or the properties of the seismic sources of the signals. We investigate the impact of the perturbations in seismic source properties on time-lapse velocity estimation. We suggest a criterion for selecting seismic events that can be used in velocity analysis. This criterion depends on the dominant frequency of the signals, the centertime of the used time window in a signal, and the estimated relative velocity change. The criterion provides a consistent framework for monitoring changes in subsurface velocities using microseismic events and an ability to assess the accuracy of the velocity estimations.

Key words: time-lapse monitoring, coda wave interferometry, microseismicity

1 INTRODUCTION

Monitoring temporal changes within the Earth's subsurface is a topic of interest in many areas of geophysics. These changes can result from an earthquake and its associated change in stress (Cheng et al., 2010), fluid injection or hydrofracturing (Davis et al., 2003), and oil and gas production (Zoback and Zinke, 2002). Some of the subsurface perturbations induced by these processes include temporal and spatial velocity changes, stress perturbations, changes in anisotropic properties of the subsurface, and fluid migration. Many of these changes span over a broad period of time and might even influence tectonic processes, such as induced seismicity (Zoback and Harjes, 1997). For example, Kilauea, Hawaii (which erupted in November 1975) is suggested to have triggered a magnitude 7.2 earthquake within a half hour of the eruption (Lipman et al., 1985). A seismic velocity perturbation of the subsurface leads to progressive time shifts across the recorded seismic signals. Various methods and data have been used to resolve the velocity perturbations. These methods include seismic coda wave interferometry (Snieder et al., 2002), doublet analysis of repeating microseismic and earthquake codas (Poupinet et al., 1984), time-lapse tomography (Vesnaver et al., 2003), and ambient seismic noise analysis (Cheng et al., 2010; Sens-Schönfelder and Wegler, 2006; Wegler and Sens-Schönfelder, 2007; Brenguier et al., 2008; Meier et al., 2010). Earthquake codas have higher sensitivity to the changes in the subsurface because multiple scattering allows these signals to sample the area of interest multiple times. However, there are inherent challenges in the use of these signals. Doublet analysis of the earthquake (microseismic) codas requires repeating events. Failure to satisfy the requirement that the events are identical can compromise the accuracy of the estimated velocity changes. In this study, we focus on the estimation of velocity changes using codas of repeating earthquakes that are not quite identical in their locations and source mechanisms.

Fluid-triggered microseismic events often are repeatable, but then events occur at slightly different positions with somewhat different source mechanisms (Sasaki and Kaieda, 2002; Godano et al., 2012). Imprints of the source perturbation and the velocity change on the seismic waveforms can be subtle, thereby retaining the similarity between seismic signals. Therefore, we will need to ask, how do the source location, source mechanism, and subsurface perturbations affect the estimated velocity changes? Snieder (2006)

shows that we can retrieve velocity changes from the coda of the waveforms recorded prior to and after the change. Robinson et al. (2011) develop a formulation using coda wave interferometry to estimate changes in source parameters of double-couple sources from correlation of the coda waves of doublets. Snieder and Vrijlandt (2005), using a similar formulation, relates the shift in the source location to the variance of the travel time perturbations between the doublet signals. In all these studies, the authors assume that the expected (average) change in travel time of the coda (due to either changes in the source locations or source mechanisms) is zero.

In this study, we investigate the impact of changes in source properties on the estimation of relative velocity changes. Knowledge of the impact of these perturbations on the estimated velocity change allows for a consistent framework for selecting pairs of earthquakes or microearthquakes used in velocity change analysis. This results in a more robust estimation of velocity change. In Section 2, we explore the theoretical relationships between the velocity changes and perturbations in the earthquake (microseismic) source properties. Following this section is a numerical validation of the theoretical results. We explain the implications and limitations of our results in Section 4. In the appendices, we explain the mathematical foundation of our results in this study.

2 MATHEMATICAL CONSIDERATION

In this section, we use the time-shifted cross-correlation (Snieder, 2002, 2006) to develop an expression for the average value of the time perturbation of scattered waves that are excited by sources with varying source properties. This perturbation is due to changes in the velocity of the subsurface and to changes in the source properties. These changes, we assume, may occur concurrently. Figure 1 is a schematic figure showing the general setup of the problem we are investigating. Two sources (S_1 and S_2) represent a microseismic doublet (repeating microseismic events). These events occur at different locations and can have different rupture patterns. We assume that these events can be described by a double couple. We investigate the ability of using the signals of these sources for time-lapse monitoring of velocity changes, assuming that these sources occur at different times. We express the signals of the two sources as unperturbed and perturbed signals, where the perturbation refers to any change in the signal due to changes within the subsurface and/or the source properties.

The unperturbed seismic signal $U(t)$ is given as

$$U(t) = A\sum_T U^{(T)}(t) \tag{1}$$

and the perturbed seismic signal $\hat{U}(t)$ is given as

$$\hat{U}(t) = \hat{A}\sum_T (1 + r^{(T)})U^{(T)}(t - t_p^T), \tag{2}$$

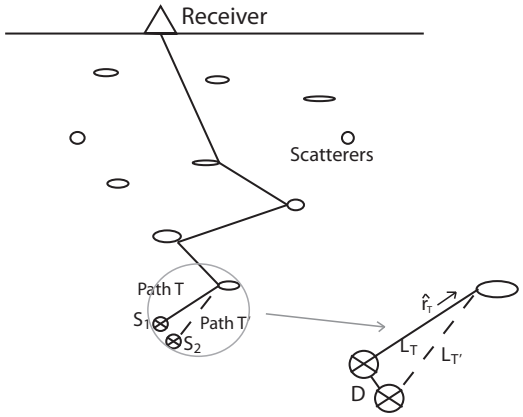

Figure 1. Geometry of wave paths. Source, S_1, produces the unperturbed signal while Source, S_2, produces the perturbed signal. Path T shows the scattering path for the unperturbed signal and the scattering path for the perturbed signal is defined by Path T'. The sources are separated by a distance D and the source distances are L_T and $L_{T'}$ distance away from the first scatterer along path T and T', respectively.

where A and $\hat{A}$ are the amplitudes of the unperturbed and perturbed source signals, respectively. These amplitudes represent the strengths of the sources. The recorded waves are a superposition of wave propagation along all travel paths as denoted by the summation over paths T. The change in the source focal mechanism only affects the amplitude of the wave traveling along each trajectory T because the excitation of waves by a double couple is real (Aki and Richards, 2002). The change in the signal amplitudes - due to changes in the source mechanism angles - is defined by $r^{(T)}$ for path T, and t_p^T is the time shift on the unperturbed signal due to the medium perturbation for path T. The change in the signal amplitudes along path T depends on the source radiation angles. In this study, we assume that the medium perturbation results from the velocity change within the subsurface and changes in the source properties. The time-shifted cross-correlation of the two signals is given as

$$C(t_s) = \int_{t-t_w}^{t+t_w} U(t')\hat{U}(t' + t_s)\,\mathrm{d}t', \tag{3}$$

where t is the centertime of the employed time window and $2t_w$ is the window length. The normalized time-shifted cross-correlation $R(t_s)$ can be expressed as follows:

$$R(t_s) = \frac{\int_{t-t_w}^{t+t_w} U(t')\hat{U}(t' + t_s)\,\mathrm{d}t'}{(\int_{t-t_w}^{t+t_w} U^2(t')\,\mathrm{d}t' \int_{t-t_w+t_s}^{t+t_w+t_s} \hat{U}^2(t')\,\mathrm{d}t')^{\frac{1}{2}}}. \tag{4}$$

As shown in appendix A, the time-shifted cross-correlation has a maximum at a time lag equal to average time perturbation ($t_s = \langle t_p \rangle$) of all waves that

arrive in the used time window:

$$\frac{1}{C(0)}\frac{\partial C(t_s)}{\partial t_s}\bigg|_{(t_s-\langle t_p\rangle)} = 0. \quad (5)$$

Equation (5) allows for the extraction of the average traveltime perturbation from the cross-correlation. In this study, the average of a quantity f is a normalized intensity weighted sum of the quantity (Snieder, 2006):

$$\langle f\rangle = \frac{\sum_T A_T^2 f_T}{\sum_T A_T^2}, \quad (6)$$

where $A_T^2 = \int U^{T2}(t')^2\,\mathrm{d}t'$ is the intensity of the wave that has propagated along path T.

We show in Appendices B and C that the expected value of the time perturbation and its variances are given by

$$\langle t_p\rangle = -\Big\langle\frac{\delta V}{V_o}\Big\rangle t \quad (7)$$

and

$$\sigma_t^2 = \langle t_p^2\rangle - \langle t_p\rangle^2 \simeq \frac{D^2}{3V_0^2}. \quad (8)$$

In the above equations, $\langle\delta V/V_0\rangle$ is the average relative velocity change, D is the shift in the source location, and V_0 is the unperturbed velocity. Equation 7 suggests that the average time shift in the multiple scattered signals results only from the velocity changes within the subsurface. The variance of the time shifts depends, however, on the perturbations of the source location.

3 NUMERICAL VALIDATION

3.1 Description of numerical experiments

We test the equations in section 2 with the numerical simulation using Foldy's multiply scattering theory (Foldy, 1945) described by (Groenenboom and Snieder, 1995). The theory models multiple scattering of waves by isotropic point scatterers. We conduct our numerical experiments using a circular 2D geometry (Figure 2) with point scatterers surrounded by 96 receiver stations. We uniformly assign the imaginary component of the scattering amplitude $|ImA| = 4$ to all the scatterers. In 2D, this is the maximum scattering strength that is consistent with the optical theorem that allows for conservation of energy (Groenenboom and Snieder, 1995). We assume an acoustic propagating wavefield which is a sum of the direct wavefield $U_0(\mathbf{r})$ and the scattered wavefield from all the scatterers:

$$U(\mathbf{r}) = U_0(\mathbf{r}) + \sum_{i=1}^{n} G^{(0)}(\mathbf{r},\mathbf{r}_i)A_iU(\mathbf{r}_i), \quad (9)$$

where the first term is the direct wave and the scattered wavefield is described by the second term. The Green's function at $\mathbf{r}$ due to scatterer i at position $\mathbf{r}_i$ is $G^{(0)}(\mathbf{r},\mathbf{r}_i)$ while $U(\mathbf{r}_i)$ is the incoming wavefield at scatterer i. The scattering amplitude of each scatterer is given by A_i. The direct wave is modulated by the far-field P-wave radiation pattern F^P:

$$U_0(\mathbf{r}) = F^P G^{(0)}(\mathbf{r},\mathbf{r}_s), \quad (10)$$

with $\mathbf{r}_s$ the source location. In 2D, where the take-off direction is restricted within the 2D plane, F^P is given as (Aki and Richards, 2002)

$$F^P = \cos\lambda\sin\delta\sin 2(\psi-\phi) - \sin\lambda\sin 2\delta\sin^2(\psi-\phi), \quad (11)$$

where ψ is the azimuth of the outgoing wave and λ, δ, and ϕ are the source parameters (rake, dip and strike, respectively). Sources are located at the center of the scattering area. The source spectrum has a dominant frequency f_d of approximately 30 Hz and a frequency range of 10-50 Hz. The source spectrum tapers off at the frequency extremes by a cosine taper with a length given by half of the bandwidth. We assume a reference velocity $V_0 = 3500$ m/s. Because the model we are using is an isotropic multiple scattering model, the transport mean free path is the same as the scattering mean free path: $l^* = l$. The scattering mean free path l^* is given by (Busch et al., 1994; Groenenboom and Snieder, 1995)

$$l^* = \frac{k_o}{\rho|ImA|}, \quad (12)$$

where k_o is the wavenumber of the scattered signal and ρ is the scatterer density. For our model, the mean free path l^* is approximately 12.2km. There is no intrinsic attenuation in the numerical model.

We generate multiple scattered signals, which are recorded at the receivers, using the numerical model in Figure 2. These signals are generated with a reference model defined by the following reference parameter values: the source radiation parameters $\phi = 0^o$, $\lambda = 0^o$, $\delta = 90^o$; change in medium velocity $\Delta V = 0$ m/s; and shift in the source location $D = 0$ m. We refer to signals generated by this reference model as the the reference signals. In order to understand the effect of the perturbation of these parameters on velocity change estimation, we also generate synthetic signals from the perturbed version of the model. The perturbed model consists of perturbation of either the source locations, source radiation parameters, the medium velocity, or a combination of these. Synthetic signals from the reference and the 0.4% velocity perturbed models are shown in Figure 3 with zoom insets showing the stretching of the waveform by the velocity perturbation. The result of the velocity perturbation on the signals is a progressive time shift of the arriving seismic phases in the signals.

3.2 Data processing

To estimate the velocity perturbations or possible velocity change imprints on the synthetic signals due to the perturbation of the source location or its radiation

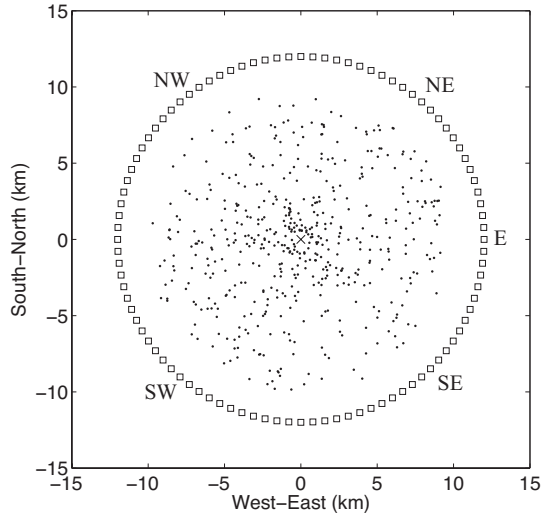

Figure 2. The experiment geometry of the numerical simulation. The receivers (squares) are surrounding the point scatterers (black dots). The source is positioned in the origin (cross). All perturbations of the source location is done from this position. The stations marked (NW, NE, E, SE, and SW) are used in the presentation of results in Figures 7 and 8.

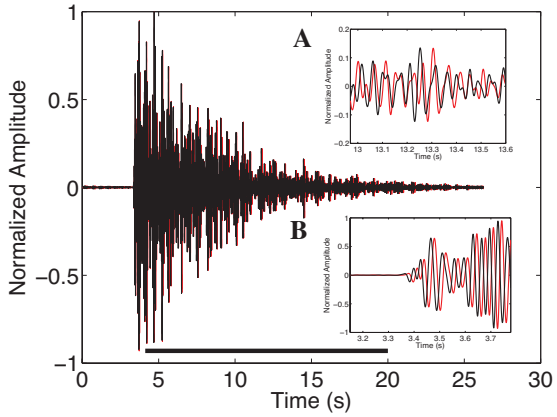

Figure 3. Recorded seismic signals at station E (Figure 2), the reference signal (red line) and the recorded signal (black line) with 0.4% relative velocity change. Inset A shows the late coda while inset B shows the first arrivals of the two signals. The black bold line is the time window used for data processing.

properties, we use the stretching algorithm of (Hadzioannou et al., 2009) who demonstrate the stability and robustness of the algorithm relative to the moving time-window cross-correlation of (Snieder et al., 2002) and the moving time-window cross-spectral analysis of (Poupinet et al., 1984). Both algorithms satisfy the relative velocity change equation (Snieder, 2006):

$$\left\langle \frac{t_p}{t} \right\rangle = -\epsilon, \tag{13}$$

where $\epsilon = \langle \delta V / V_o \rangle$ is the relative velocity change.

In the stretching algorithm, we multiply the time of the perturbed signal with a stretching factor $(1-\epsilon)$ and interpolate the perturbed signal at this stretched time. The time window we use in all our analysis is given by the black bold line in Figure 3. We then stretch the perturbed signal at a regular interval of ϵ values. The range of the ϵ values can be arbitrarily defined or predicted by prior information on the range of changes in the subsurface velocity. To resolve the value of ϵ, we use an L_2 objective function rather than the cross-correlation algorithm as suggested by (Hadziioannou et al., 2009). For events of equal magnitude ($A = \hat{A}$), the objective function is

$$R(\epsilon) = ||\hat{U}(t(1-\epsilon)) - U(t)||_2, \tag{14}$$

where $||...||_2$ is the L_2 norm. Figure 4 shows the objective function for the case of a 0.4% velocity change. The minimum of the objective function depends on the amplitude changes between the two signals and on the travel time perturbations due to velocity changes and shifts in the source location. The signals have uniform magnitudes. The amplitude changes between the signals are due to changes in the orientation of the source angles.

The error in the estimated relative velocity change $e_{\delta v}$ is given by

$$e_{\delta v} \leq \frac{\sigma_U}{2\pi f_d A t}, \tag{15}$$

where f_d is the dominant frequency, t is the centertime of the signal, A is the amplitude of the signals, and σ_U is the standard deviation of the recorded waveforms. The derivation of the error equation (equation 15) is given in Appendix D. The error associated with the velocity change depends on additive noise in the signals and on differences in the signals both in amplitude and in phase due to perturbation in source properties.

3.3 Effect of perturbation of source properties on the estimated velocity change

To understand the effect of the changes in the source properties on the estimation of the relative velocity changes, we conduct our numerical experiment over a range of parameter changes. We perturb the source location and the orientation of the source angles. The perturbation of the source radiation parameters is characterized by the weighted root mean square change in source parameters $\langle r \rangle$ (Robinson et al., 2007):

$$\langle r \rangle = -\frac{1}{2}(4\Delta\phi^2 + \Delta\lambda^2 + \Delta\delta^2), \tag{16}$$

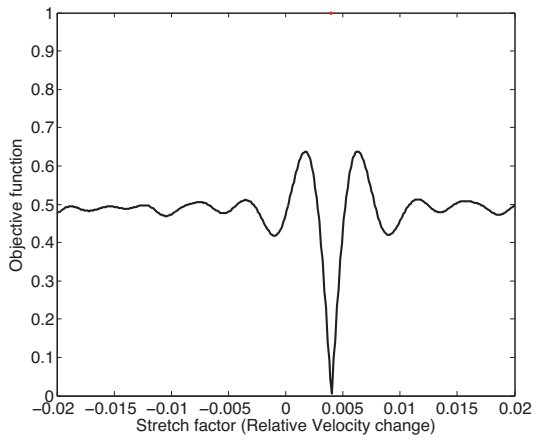

Figure 4. The objective function $R(\epsilon)$ as a function of the stretch factor ϵ. The objective function is minimum for ϵ = 0.4%, which corresponds to the time velocity change.

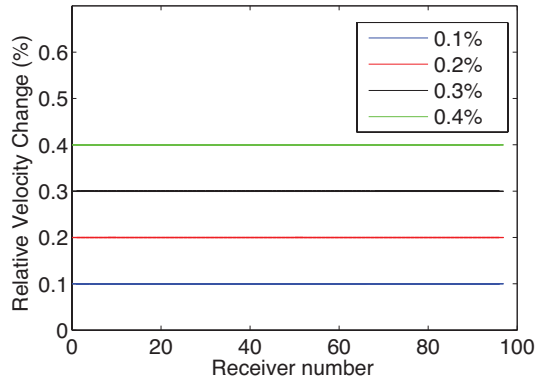

Figure 5. Estimated relative velocity change for model velocity change of $\langle \frac{\delta V}{V_0} \rangle$ = 0.1% (blue), $\langle \frac{\delta V}{V_0} \rangle$ = 0.2% (red), $\langle \frac{\delta V}{V_0} \rangle$ = 0.3% (black), and $\langle \frac{\delta V}{V_0} \rangle$ = 0.4% (green).

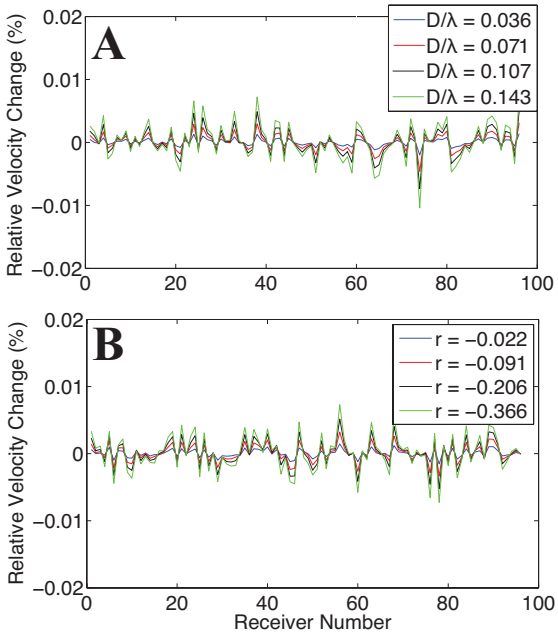

Figure 6. Estimated relative velocity change due to perturbation in the source location and the source radiation. A. The estimated velocity change for perturbed source location (divided by the dominant wavelength; inset in the top right) and B. The estimated velocity change caused by changes in source radiation angles (inset in the top right). The value of r is given by equation 14.

where $\Delta\phi$ is the change in strike, $\Delta\lambda$ is the change in rake, and $\Delta\delta$ is the change in dip. These changes represent the angle differences between the two sources (doublet).

Figures 5 and 6 show the estimated velocity changes due to the perturbation of medium velocity and the source properties (location and radiation parameters), respectively. For Figure 5, we generate signals with the following perturbation in the model velocity $\langle \delta V/V_0 \rangle$: 0.1%, 0.2%, 0.3%, and 0.4%. In these models, we keep the source parameters unchanged. Using the stretching method, we are able to recover the velocity changes we impose in the model from the codas of each of the perturbed signals and that of the reference signal (Figure 5). The method accurately estimates the model velocity change in all the recievers. We also generate signals with only perturbations in the source locations and mechanisms. In this case, the true velocity change is zero. Figure 6 shows that the estimated relative velocity changes $\langle \delta V/V_o \rangle$ are near the true value ($\delta V = 0$) for models with perturbations of either the source location or the source radiation parameters. The velocity change estimated from individual stations varies around zero, but with a shift in the source location of $D = 0.143\lambda_d$, with λ_d the dominant wavelength and source angle perturbations as large as $\Delta\phi = 20^o$, $\Delta\lambda = 20^o$, and $\Delta\delta = 20^o$ ($\langle r \rangle$ = -0.366), the magnitude of these variations is smaller than 1/20th of the typical velocity changes inferred from seismic signals (Figure 6). These variations in the velocity change inferred from different stations can be used to estimate the errors in the estimated velocity change. These results agree with equation (7) which predicts that the average value of time shifts in the perturbed signal results only from changes in the medium velocity and is not affected by changes in source properties. We will need to know how effectively we can resolve the velocity changes in our model in the presence of the other model parameter perturbations.

3.4 Limiting regimes of the estimations

To investigate the extent of the perturbation in the source location and source radiation perturbations that can be allowed in the estimation of relative velocity changes, we generate synthetic signals with models having a 0.1% relative velocity change and various perturbations of the source parameters. The values of the source parameter perturbations are given in Tables 1 and 2. Figure 7 shows the estimated relative velocity changes from signals generated from sources at different locations. The figure shows that we can recover the model relative velocity change of 0.1% using doublets (two sources) within a sphere of radius $\lambda_d/4$, where λ_d is the dominant wavelength of the seismic signal which is approximately 140 m. This is consistent with the criterion we derived in Appendix E, which predicts that for an accurate estimation of the subsurface velocity change, the shift in the source location has to satisfy

$$\frac{D}{\lambda_d} < \sqrt{2}\left|\left\langle \frac{\delta V}{V_o} \right\rangle\right| f_d t, \tag{17}$$

where f_d is the dominant frequency of the signals, $\langle \delta V/V_0 \rangle$ is the average velocity change in the subsurface, and t is the centertime of the processed signal. The criterion is derived from a comparison of the phase changes due to velocity changes with those due to shifts in the source location. For the results in Figure 7, our model parameters are $\langle \delta V/V_o \rangle = 0.001$, $t = 10$s, and $f_d \simeq 25$Hz. With these values, the constraint on the source location shift for Figure 7 is

$$\frac{D}{\lambda_d} < 0.35. \tag{18}$$

Figure 7 shows that for $D/\lambda_d \geq 0.3$, the estimated velocity change deviates significantly from the real velocity change; this is in agreement with equation (18). The criterion in equation (17) imposes a constraint on the spacing requirements for the source locations of the doublets used for time-lapse velocity change monitoring with microearthquakes. Alternatively, equation (17) gives the magnitude of a velocity change that is resolvable with a given shift in the source location. According to equation (17), the allowable source separation increases with the centertime t of the employed time window. This is due to the fact that the imprint of the velocity change is more pronounced as the waves have propagated over a greater distance through the perturbed medium. However, signals at later times in the coda are more affected by the presence of additive noise because the signal-to-noise ratio usually decreases towards the late coda.

We also investigate the effect of the source radiation properties on the estimated velocity change of the medium of interest. Figure 8 shows the estimated velocity changes from a model with 0.1% velocity change using sources with perturbed radiation angles (measured by $\langle r \rangle$). The values of the perturbed source radiation angles are given in Table 2. In Figure 8A, the estimated

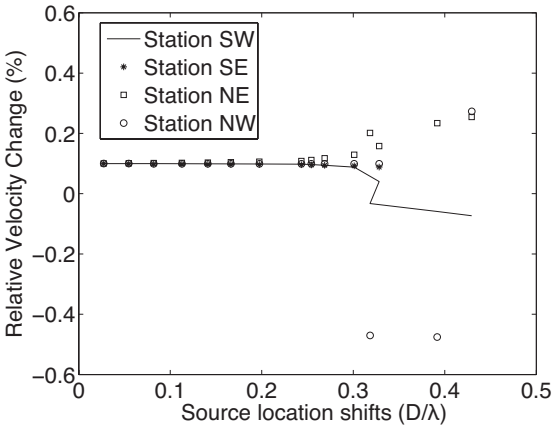

Figure 7. Estimated relative velocity change after a 0.1% velocity change and various source location perturbations (Table 1). The shift in the source locations are divided by the dominant wavelength λ_d of the recorded signals. For values of the source location shift greater than $\frac{1}{4}\lambda_d$, we have incorrect estimates for the velocity change due to the distortion of the perturbed signal. Stations SW, SE, NE, and NW positions are given in Figure 2.

Table 1. Modeling parameters for shift in the source location.

Case	$\frac{\Delta V}{V}$	D (λ_d)
Reference	0	0
Case 1	0.1	0.0274
Case 2	0.1	0.0547
Case 3	0.1	0.0820
Case 4	0.1	0.1094
Case 5	0.1	0.1367
Case 6	0.1	0.1642
Case 7	0.1	0.1918
Case 8	0.1	0.2197
Case 9	0.1	0.2477
Case 10	0.1	0.2760
Case 11	0.1	0.3047
Case 12	0.1	0.3337
Case 13	0.1	0.3627
Case 14	0.1	0.3916
Case 15	0.1	0.4202

Table 2. Modeling parameters for source radiation perturbation.

Case	$\frac{\Delta V}{V}$	$\Delta\phi(^o)$	$\Delta\lambda(^o)$	$\Delta\delta(^o)$	-$\langle r\rangle$
Reference	0	0	0	0	0
Case 1	0.1	0	0	0	0
Case 2	0.1	2	2	2	0.0037
Case 3	0.1	4	4	4	0.0146
Case 4	0.1	6	6	6	0.0329
Case 5	0.1	8	8	8	0.0585
Case 6	0.1	10	10	10	0.0914
Case 7	0.1	12	12	12	0.1316
Case 8	0.1	14	14	14	0.1791
Case 9	0.1	16	16	16	0.2339
Case 10	0.1	18	18	18	0.2961
Case 11	0.1	20	20	20	0.3655
Case 12	0.1	22	22	22	0.4423
Case 13	0.1	24	24	24	0.5264
Case 14	0.1	26	26	26	0.6178
Case 15	0.1	28	28	28	0.7165

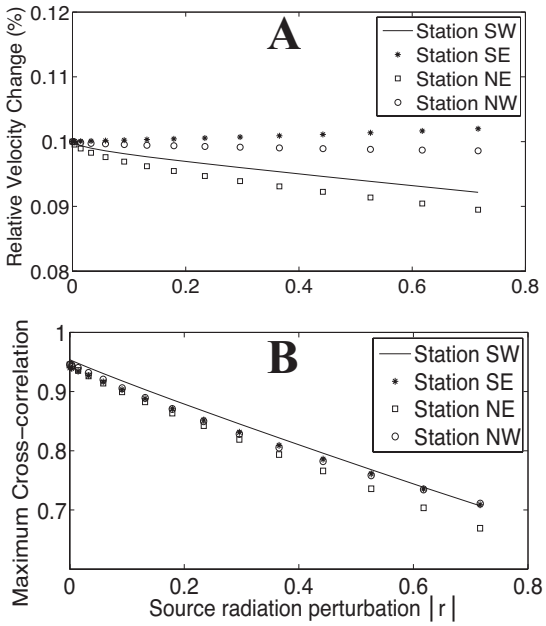

Figure 8. Effect of source angle perturbation on estimated velocity change. A. The estimated relative velocity changes are from a 0.1% model velocity change and various source radiation perturbations (Table 2). B. The decorrelation of the doublets, due to source angle perturbations, measured by maximum cross-correlation values. Stations SW, SE, NE, and NW positions are given in Figure 2.

velocity change at the individual stations progressively deviates from the true velocity change of 0.1% with increasing change in the orientations of the source angles. This deviation is due to the decorrelation between the perturbed and the unperturbed signals as shown in Figure 8B, which shows the maximum normalized cross-correlation of the codas within the processed time window. With an increasing change in the orientation of the sources, the maximum cross-correlation value of the waves excited by the doublets decreases. However, for source angle perturbations as large as $\Delta\phi = 28^o$, $\Delta\lambda = 28^o$, and $\Delta\delta = 28^o$ corresponding to $|\langle r\rangle| = 0.72$ (Figure 8A), the maximum deviation from the 0.1% model velocity change is approximately 0.01%. This is a small change compared to velocity changes resolved from seismic signals in practice. The maximum cross-correlation (Figure 8B) can be retrieved from the data and can be used as a diagnostic of the accuracy of the estimated velocity change. In this example, a maximum cross-correlation of 0.7 indicates an error of about 10% in the estimated velocity change.

4 DISCUSSION AND CONCLUSION

In this study, we investigate the influence of perturbation in source properties (location and radiation) on the estimation of velocity changes. These velocity changes are extracted from multiply scattered signals (codas) of repeating events. We show that we can resolve accurate values of relative velocity changes if the shift in the source location satisfies the constraint (equation 17). This constraint depends on the dominant frequency of the signal, the estimated relative velocity change, and the centertime of the employed time window. This places a restriction on the relative event locations that can be used to estimate the relative velocity change of the subsurface. However, to use this constraint, we need to know the magnitude of the relative velocity change we seek to measure. Preliminary results on the velocity change can be used to pick events satisfying equation (17) for an accurate estimation of the velocity changes. Using doublets that do not satisfy the constraint result to an inaccurate estimate of the velocity change.

A significant change in the source mechanism of double couple sources can introduce a bias in the estimation of relative velocity change. This bias is due to the decorrelation of the perturbed and unperturbed signals which lowers the accuracy of the estimated velocity change. As shown in Figures 6B and 8A, some of the stations underestimate while others overestimate the velocity change. However, this bias is negligible for the typical velocity changes resolved from seismic signals in practice. This result permits the use of sources

of different orientations for the estimation of velocity changes, provided that the maximum cross-correlation of the source signals is greater than 0.7 as shown in Figure 8B. For a consistent estimate of the velocity change, using multiple stations is useful to ascertain the accuracy of the estimated velocity change in an isotropic subsurface.

The theory presented in this study is based on a number of simplifications and assumptions. First, we assume a uniform velocity change across our model. For the case of a localized isotropic velocity change, the resolved velocity change is a fraction of the local velocity change, where the fraction is dependent on the amount of time the codas spend within the perturbed region relative to the unperturbed region. Also, we assume that the velocity is isotropic. In an anisotropic velocity medium, we need to include the dependence of the velocity on the direction of propagation.

In this study, we assume that the scatterer density is uniform in all directions from the source. We also ignore changes in the scattering properties which might include shifts in scatterer locations (Niu et al., 2003) and changes in the scattering strength of the scatterers. These changes in the scatterer properties can be due to changes in fluid properties such as fluid migration or opening and closing of fractures and pre-existing faults. If the shifts in the scatterer location are random, the average travel time perturbation due to scatterer location shift is zero. However, if the shifts in the scatterer locations are non-random or directional, the average time perturbation due to scatterer location shift over all take-off angles is a non-zero mean traveltime change. A non-zero mean traveltime perturbation is also expected for non-uniform scatterer density. The scattered signals lag behind while traveling through a higher scatterer density region compared to a lower scatterer density region. These introduce a bias in the estimated relative velocity changes if the changes in scatterer properties or density are significant.

We used point scatterers in our numerical modeling even though in the real world, scattering can be caused by faults, fractures, horizontal or dipping layers. The employed modeling uses scalar waves, hence it does not account for mode conversions of elastic waves (for example, P-to-S or S-to-P and surface waves) that might result due to the presence of layers, free surface, and fractures. The coda is usually dominated by S wave (Aki and Chouet, 1975; Snieder, 2002), hence the mode conversions between P and S waves do not dominate the details of the scattering processes.

APPENDIX A: EXTRACTING TIME SHIFT FROM THE CROSS-CORRELATION

This appendix shows the extraction of the average time perturbation from the time-shifted cross-correlation. Using the time-shifted cross-correlation, we show that the maximum value of the cross-correlation occurs at a time lag which is equal to the average time perturbation resulting from changes either in the subsurface velocity, source locations, or source focal mechanisms. Re-expressing time-shifted cross correlation function (equation (3)) gives

$$C(t_s) = \sum_T (1+r^{(T)}) \int_{t-t_w}^{t+t_w} (U^T(t')U^T(t'+t_s-t_p^T))\,\mathrm{d}t'. \tag{A1}$$

The time-shifted cross-correlation has double sum contributions from the diagonal terms $\sum_{T=T'}$ and the crossterms $\sum_{T\neq T'}$ due to the product of $\hat{U(t)}$ and $U(t)$ which individually involve summation over all trajectories. The summation in equation A1, only accounts for the contributions from the diagonal terms ($\sum_{T,T'} = \sum_{T=T'} + \sum_{T\neq T'} \rightarrow \sum_{T=T'}$), because we ignore the crossterms $\sum_{T\neq T'}$. The crossterms depend on the bandwidth of the signals Δf and the length of the cross-correlation window $2t_w$ (Snieder, 2006):

$$\frac{|\text{crossterms}|}{|\text{diagonal terms}|} = \sqrt{\frac{1}{\Delta f 2t_w}}. \tag{A2}$$

The crossterms become negligible with an increasing length of time window used for the time window.

Using a Taylor's series expansion of $U^T(t'+t_s-t_p^T)$ in $t_s - t_p^T$,

$$C(t_s) = \sum_T (1+r^{(T)}) \int_{t-t_w}^{t+t_w} \left(U^T(t')^2 + \frac{(t_s-t_p^T)}{2} U^T(t')\dot{U}^T(t') + \frac{(t_s-t_p^T)^2}{2} U^T(t')\ddot{U}^T(t') \right) \mathrm{d}t'. \tag{A3}$$

The contribution of the first time derivative $\dot{U}^T(t')$ term can be reduced on the end-points contributions of the signals. Since we taper the windowed coda to eliminate edge effects these end-point contributions vanish:

$$\int_{t-t_w}^{t+t_w} (t_s - t_p^T) U^T(t')\dot{U}^T(t')\,\mathrm{d}t' = \frac{1}{2} U^{T2}(t)\Big|_{t-t_w}^{t+t_w} = 0, \tag{A4}$$

because the tapered signals at the end-points are zero (Snieder, 2006). Using integration by parts, equation A3 can be re-expressed as

$$C(t_s) = \sum_T (1+r^{(T)}) \times \int_{t-t_w}^{t+t_w} (U^T(t')^2 - \frac{(t_s-t_p^T)^2}{2} \dot{U}^T(t')^2)\,\mathrm{d}t'. \tag{A5}$$

The time-shifted cross correlation is maximum when it's first derivative with respect to the lagtime t_s is zero. The first derivative of the cross-correlation function with re-

spect to t_s is given as

$$\frac{\partial C(t_s)}{\partial t_s} = -\sum_T (1 + r^{(T)})(t_s - t_p^T) \int_{t-t_w}^{t+t_w} (\dot{U}^T(t')^2)\, \mathrm{d}t'. \tag{A6}$$

Using $C(0) = \sum_T \int_{t-t_w}^{t+t_w} U^T(t')^2\, \mathrm{d}t'$, the normalized derivative of the time-shifted cross-correlation is given by

$$\frac{1}{C(0)}\frac{\partial C(t_s)}{\partial t_s} = - \frac{\sum_T (1 + r^{(T)})(t_s - t_p^T) \int_{t-t_w}^{t+t_w} (\dot{U}^T(t')^2)\, \mathrm{d}t'}{\sum_T \int_{t-t_w}^{t+t_w} (U^T(t')^2)\, \mathrm{d}t'}. \tag{A7}$$

We next define the mean frequency $\bar{\omega}^2$ as

$$\bar{\omega}^2 = \frac{\sum_T \int_{t-t_w}^{t+t_w} (\dot{U}^T(t'))^2\, \mathrm{d}t'}{\sum_T \int_{t-t_w}^{t+t_w} (U^T(t'))^2\, \mathrm{d}t'}. \tag{A8}$$

Therefore, using equation (6)

$$\frac{1}{C(0)}\frac{\partial C(t_s)}{\partial t_s} = -\frac{\sum_T A_T^2 (1 + r^{(T)})(t_s - t_p^T)\bar{\omega}^2}{\sum_T A_T^2}. \tag{A9}$$

We assume that the amplitude perturbations due to the change in the source mechanism and the traveltime perturbations are independent. In that case, using equation 6, equation A9 becomes

$$\frac{1}{C(0)}\frac{\partial C(t_s)}{\partial t_s} = -(1 + \langle r \rangle)(t_s - \langle t_p \rangle)\bar{\omega}^2. \tag{A10}$$

The right hand side vanishes when

$$t_s - \langle t_p \rangle = 0. \tag{A11}$$

This shows that the time shift t_s where the cross-correlation is maximum is the average of the travel-time perturbations.

APPENDIX B: THE TIME PERTURBATION DUE TO A PERTURBED SOURCE

From Figure 1, the traveltime t_T for the signal along path T from the unperturbed source to the first scatterer along path T is given by

$$t_T = \frac{L_T}{V_o}, \tag{B1}$$

where V_o is the unperturbed medium velocity. Also the traveltime $t_{T'}$ for the signal along path T' from the perturbed source to the same first scatterer is given by

$$t_{T'} = \frac{L_{T'}}{V}. \tag{B2}$$

We assume that the signals from both sources after scattering by the first scatterer travel along the same path (Figure 1). We define $L_T = L_{T'} + \delta L$ and $V = V_o + \delta V$, where $\delta L = -(\hat{\mathbf{r}}_T \cdot \mathbf{D})$, with $\mathbf{D}$ the perturbation of the source location and $\hat{\mathbf{r}_T}$ the take-off direction from the first source to the scatterer. The takeoff direction from the source $\hat{\mathbf{r}}_T$ in spherical coordinates is

$$\hat{\mathbf{r}}_T = \begin{pmatrix} \cos\psi \sin\theta \\ \sin\psi \sin\theta \\ \cos\theta \end{pmatrix}, \tag{B3}$$

where ψ and θ are colatitude and longitude in spherical coordinates. The traveltime for the signal along path T from the second source to the first scatterer can be re-expressed as

$$t_{T'} = \frac{L_{T'}}{V_o + \delta V} \tag{B4}$$

$$\simeq \left(\frac{1}{V_o} - \frac{\delta V}{V_o^2} + ...\right) L_T - \left(\frac{1}{V_o} - \frac{\delta V}{V_o^2} + ...\right) \cdot (\hat{\mathbf{r}}_T \cdot \mathbf{D}). \tag{B5}$$

Ignoring the terms of second order or higher, equation B5 gives,

$$t_{T'} \simeq \frac{L_T}{V_o} - \left(\frac{\delta V}{V_o}\right)\left(\frac{L_T}{V_o}\right) - \frac{(\hat{\mathbf{r}}_T \cdot \mathbf{D})}{V_o}, \tag{B6}$$

$$= t_T + t_{pv} + t_{pl}. \tag{B7}$$

Therefore, the time perturbation along path T' is given as

$$t_p^{T'} = t_{T'} - t_T = t_{pv} + t_{pl}, \tag{B8}$$

where t_{pv} = time shift due to velocity change and t_{pl} = time shift due to shift in source .

We need to derive the expression for $\langle t_p \rangle$. With equation 6 and equation B8, the average time perturbation is given,

$$\langle t_p \rangle = \frac{\sum_T A_T^2 t_p^T}{\sum_T A_T^2} = \frac{-\sum_T A_T^2 \left((\frac{\delta V}{V_o})(\frac{L_T}{V_o}) + (\frac{\hat{\mathbf{r}}_T \cdot \mathbf{D}}{V_o}) \right)}{\sum_T A_T^2},$$

$$= \left\langle \frac{\delta V}{V_o} \right\rangle \frac{\int_T L_T/V_o\, \mathrm{d}\Omega}{\int_T \mathrm{d}\Omega} + \frac{\int_T (\hat{\mathbf{r}}_T \cdot \mathbf{D})/V_o\, \mathrm{d}\Omega}{\int_T \mathrm{d}\Omega}, \tag{B9}$$

where $\int_T ... \mathrm{d}\Omega$ denotes an integration over all take-off angles. In 3D, the integration limits of $\mathrm{d}\theta$ and $\mathrm{d}\psi$ are $[0, \pi]$ and $[0, 2\pi]$, respectively. Since $\int_T \hat{\mathbf{r}}_T\, \mathrm{d}\Omega = 0$ and $\int_T L_T/V_o\, \mathrm{d}\Omega / \int_T \mathrm{d}\Omega = t$, where t is the traveltime of the scattered ray from the source to the receiver along path T, equation B9 reduces to

$$\langle t_p \rangle = -\left\langle \frac{\delta V}{V_o} \right\rangle t. \tag{B10}$$

Hence to first order in D, the average traveltime perturbation depends only on the velocity changes within the explored medium.

APPENDIX C: VARIANCE OF TIME PERTURBATION

The variance of the travel time perturbation, using equation 6, is given by

$$\sigma_t^2 = \frac{\sum_T A_T^2 (t_p - \langle t_p \rangle)^2}{\sum_T A_T^2} = \langle t_p^2 \rangle - \langle t_p \rangle^2. \quad \text{(C1)}$$

where using expression B-8 $\langle t_p^2 \rangle$ is given by

$$\langle t_p^2 \rangle = \frac{\sum_T A_T^2 \left(-\left(\frac{\delta V}{V_o}\right)\left(\frac{L_T}{V_o}\right) - \frac{\hat{\mathbf{r}}_T \cdot \mathbf{D}}{V_o} \right)^2}{\sum_T A_T^2}. \quad \text{(C2)}$$

Expanding equation (C2) gives

$$\langle t_p^2 \rangle = \sum_T A_T^2 \left(\left(\frac{\delta V}{V_o}\right)^2 \left(\frac{L_T}{V_o}\right)^2 + \left(\frac{\hat{\mathbf{r}}_T \cdot \mathbf{D}}{V_o}\right)^2 \right.$$

$$\left. + 2\left(\frac{\delta V}{V_o}\right)\left(\frac{L_T}{V_o}\right)\left(\frac{\hat{\mathbf{r}}_T \cdot \mathbf{D}}{V_o}\right) \right) \Big/ \sum_T A_T^2. \quad \text{(C3)}$$

In equation (C3),

$$\frac{\int_T (\hat{\mathbf{r}}_T \cdot \mathbf{D})^2 \, \mathrm{d}\Omega}{\int_T \mathrm{d}\Omega} = \frac{D^2}{C}, \quad \text{(C4)}$$

where C = 1,2,or 3 which specifies the dimension of the problem. Therefore, in 3D,

$$\langle t_p^2 \rangle = \left\langle \frac{\delta V}{V_0} \right\rangle^2 t^2 + \frac{D^2}{3V_0^2}, \quad \text{(C5)}$$

Combining equations (C5) and (B10), the total variance of the time perturbation is

$$\sigma_t^2 = \frac{D^2}{3V_0^2}. \quad \text{(C6)}$$

In the absence of additive noise, the variance of the traveltime perturbation thus depends only on the shift in the source location. With the estimate of the subsurface velocity, we can estimate the shift in the source location from equation C6.

APPENDIX D: ERROR ESTIMATION

We estimate the error associated with the estimated relative velocity change using the data residuals from the L_2 norm. Using a Taylor series expansion of $\hat{U}(t + t_p)$ in t_p,

$$\hat{U}(t + t_p) \simeq U(t)(1 - i\omega_d t_p) \quad \text{(D1)}$$

where ω_d is the $2\pi f_d$ with f_d the dominant frequency of the signal. Including additive errors $\delta U(t)$ in the data with standard deviation σ_U, equation D1 gives

$$\hat{U}(t + t_p) + \delta U(t) \simeq U(t)(1 - i2\pi f_d(t_p + \delta t)). \quad \text{(D2)}$$

where δt is the error of the traveltime perturbation due to the error in the data $\hat{U}(t+t_p)$. This error leads to an error in the estimated lagtime from the cross-correlation of the perturbed and unperturbed signals. Therefore, the relationship between the data error and the error in the time perturbation is

$$\sigma_U \simeq -iU(t)2\pi f_d \sigma_t. \quad \text{(D3)}$$

where σ_t is the standard deviation of the error in the traveltime perturbation. Therefore, the error in the time perturbation between the perturbed and unperturbed signals is

$$\sigma_t = ||\hat{t_p} - t_p||_2 \leq \frac{\sigma_U}{||M||_2}, \quad \text{(D4)}$$

where $\hat{t_p}$ and t_p are the estimated and the exact time perturbations, respectively, and the M is $-iU(t)2\pi f_d$. Combining equations 7 and D4, the error in the estimated relative velocity change $e_{\delta v}$ is the time-normalized time perturbation error

$$e_{\delta v} = \frac{\sigma_t}{t} \leq \frac{\sigma_U}{||U||_2 2\pi f_d t}. \quad \text{(D5)}$$

In practice, t is the centertime of the used time window, $||U||_2$ is the amplitude of the data.

The error equation (equation D5) depends on the dominant frequency of the signal, the length of the signals, and the amplitude difference between the signals $\hat{U(t)}$ and $U(t)$ which is normalized by the amplitude of $U(t)$. The error in the data σ_U is due to any dissimilarity between the two signals $\hat{U(t)}$ and $U(t)$ resulting from either shift in the source location or the presence of additive noise.

APPENDIX E: COMPARATIVE TIME SHIFT BETWEEN CHANGES IN VELOCITY AND SOURCE LOCATION

In this section, we compare phase shifts due to the shift in the source location to the phase shifts resulting from velocity change within the subsurface. If the phase of the wave that travels over a distance r from a source to a scatterer is $\exp(i\mathbf{k} \cdot \mathbf{r}_T)$, the phase change due to shift in the source location along path T is

$$\exp(-ik(\hat{\mathbf{r}}_T \cdot \mathbf{D})) = \exp(-ikD\cos\theta_T), \quad \text{(E1)}$$

where θ_T is the angle between the take-off ray of path T and the shift in the source location D, and $k = 2\pi/\lambda$. For $D/\lambda < 1$, we can approximate equation E-1 as

$$\exp(-ikD\cos\theta_T) \simeq 1 - ikD\cos\theta_T - \frac{1}{2}(kD\cos\theta_T)^2. \quad \text{(E2)}$$

The average value of the phase changes due to the shift in the source location is

$$\langle \exp(-ikD\cos\theta_T) \rangle \simeq$$
$$1 - ikD\langle\cos\theta_T\rangle - \frac{1}{2}(kD)^2\langle\cos^2\theta_T\rangle, \quad \text{(E3)}$$

where $\langle \cos\theta_T \rangle = 0$, assuming we sum over all angles. For equal contribution from all take-off angles in 2D (the numerical simulations in section 3 are in 2D), $\langle \cos^2\theta_T \rangle = \frac{1}{2}$. Therefore,

$$\langle \exp(-ikD\cos\theta_T) \rangle \simeq 1 - \frac{1}{4}k^2D^2. \quad \text{(E4)}$$

Also, if the phase of the wave that travels over a time t is $\exp(-i\omega t)$, the phase change due to the change in the medium velocity is

$$\exp(-i\omega\Delta t) \simeq 1 - i\omega\Delta t - \frac{1}{2}(\omega\Delta t)^2, \quad \text{(E5)}$$

where Δt is the time shift due to velocity change. The second order terms contribute to the variance of the phase change. Therefore, for an accurate estimation of the velocity change,

$$\frac{1}{4}k^2D^2 < \frac{1}{2}\omega^2\Delta t^2. \quad \text{(E6)}$$

Equation E-6 implies that

$$\frac{D}{\lambda} < \sqrt{2}f|\Delta t|. \quad \text{(E7)}$$

But the average value of time shift due to velocity change $\langle \Delta t \rangle$ is

$$\langle \Delta t \rangle = -\Big\langle \frac{\delta V}{V_o} \Big\rangle t. \quad \text{(E8)}$$

Therefore, equation (E-7) reduces to

$$\frac{D}{\lambda} < \sqrt{2}f\Big|\Big\langle \frac{\delta V}{V_o} \Big\rangle\Big| t. \quad \text{(E9)}$$

Equation E9 shows that for an accurate estimation of relative velocity changes, the shift in the source location D has to satisfy equation E9. For practical purposes, λ and f can be defined as the dominant wavelength and frequency of the processed signal, respectively. Also, t can be assigned as the centertime of the used time window.

ACKNOWLEDGMENTS

We are grateful for the financial support of the Department of Energy (DOE) through grant DE-EE0002758.

REFERENCES

Aki, K. and L. Chouet, 1975, Origin of coda waves: source, attenuation, and scattering effects: J. Geophys. Res., **80**, 3322–3342.

Aki, K. and P. G. Richards, 2002, Quantitative seismology: University Science Books.

Brenguier, F., M. Campillo, C. Hadziioannou, N. Shapiro, and E. Larose, 2008, Postseismic relaxation along the San Andreas Fault at Parkfield from continuous seismological observations: Science, **321**, 1478–1481.

Busch, K., C. M. Soukoulis, and E. N. Economou, 1994, Transport and scattering mean free paths of classical waves: Physical Review B, **50**, 93–98.

Cheng, X., F. Niu, and B. Wang, 2010, Coseismic velocity change in the rupture zone of the 2008 Mw7.9 Wenchuan earthquake observed from ambient seismic noise: Bulletin of the Seismological Society of America, **100**, 2539 –2550.

Davis, T. L., M. J. Terrell, R. D. Benson, R. Cardona, R. R. Kendall, and R. Winarsky, 2003, Multicomponent seismic characterization and monitoring of the CO_2 flood at Weyburn Field, Saskatchewan: The Leading Edge, **22**, 696 –697.

Foldy, L. L., 1945, The multiple scattering of waves. i. general theory of isotropic scattering by randomly distributed scatterers: Physical Review, **67**, 107–119.

Godano, M., T. Bardainne, M. Regnier, A. Deschamps, and M. Valette, 2012, Spatial and temporal evolution of a microseismic swarm induced by water injection in the ArkemaVauvert salt field (Southern France): Geophysical Journal International, **188**, 274–292.

Groenenboom, J. and R. Snieder, 1995, Attenuation, dispersion, and anisotropy by multiple scattering of transmitted waves through distributions of scatterers: The Journal of the Acoustical Society of America, **98**, 3482–3492.

Hadziioannou, C., E. Larose, O. Coutant, P. Roux, and M. Campillo, 2009, Stability of monitoring weak changes in multiply scattering media with ambient noise correlation: Laboratory experiments: The Journal of the Acoustical Society of America, **125**, 3688–3695.

Lipman, P., J. Lockwood, R. Okamura, D. Swanson, and K. Yamashita, 1985, Ground deformation associated with the 1975 magnitude-7.2 earthquake and resulting changes in activity of Kilauea volcano, Hawaii: U.S. Geological Survey Professional Paper 1276, 45.

Meier, U., S. N.M., and F. Brenguier, 2010, Detecting seasonal variations in seismic velocities within Los Angeles basin from correlations of ambient seismic noise: Geophys. J. Int., **181**, 985–996.

Niu, F., P. Silver, R. Nadeau, and T. McEvilly, 2003, Migration of seismic scatterers associated with the 1993 Parkfield aseismic transient event: Nature, **426**, 544–548.

Poupinet, G., W. L. Ellsworth, and J. Frechet, 1984, Monitoring velocity variations in the crust using earthquake doublets: An application to the Calaveras fault, California: Journal of Geophysical Research, **89**, 5719–5731.

Robinson, D. J., M. Sambridge, and R. Snieder, 2011, A probabilistic approach for estimating the separation between a pair of earthquakes directly from their coda waves: Journal of Geophysical Research, **116**, B04309, doi:10.1029/2010JB007745.

Robinson, D. J., R. Snieder, and M. Sambridge, 2007, Using coda wave interferometry for estimating the

variation in source mechanism between double couple events: Journal of Geophysical Research, **112**, B12302, doi:10.1029/2007JB004925.

Sasaki, S. and H. Kaieda, 2002, Determination of stress state from focal mechanisms of microseismic events induced during hydraulic injection at the Hijiori hot dry rock site: Pure and Applied Geophysics, **159**, 489–516.

Sens-Schönfelder, C. and U. Wegler, 2006, Passive image interferometry and seasonal variations at Merapi volcano, Indonesia: Geophys. Res. Lett., **33**, L21302, doi:10.1029/2006GL027797.

Snieder, R., 2002, Coda wave interferometry and the equilibration of energy in elastic media: Physical Review E, **66**, 046615.

———, 2006, The theory of coda wave interferometry: Pure and Applied Geophysics, **163**, 455–473.

Snieder, R., A. Grêt, H. Douma, and J. Scales, 2002, Coda wave interferometry for estimating nonlinear behavior in seismic velocity: Science, **295**, 2253 –2255.

Snieder, R. and M. Vrijlandt, 2005, Constraining the source separation with coda wave interferometry: Theory and application to earthquake doublets in the hayward fault, california: Journal of Geophysical Research, **110**.

Vesnaver, A. L., F. Accaino, G. Bohm, G. Madrussani, J. Pajchel, G. Rossi, and G. D. Moro, 2003, Time-lapse tomography: Geophysics, **68**, 815 –823.

Wegler, U. and C. Sens-Schönfelder, 2007, Fault zone monitoring with passive image interferometry: Geophys. J. Int., **168**, 1029–1033.

Zoback, M. and J. Zinke, 2002, Production-induced normal faulting in the Valhall and Ekofisk oil fields: Pure and Applied Geophysics, **159**, 403–420.

Zoback, M. D. and H. Harjes, 1997, Injection-induced earthquakes and crustal stress at 9 km depth at the KTB deep drilling site, Germany: Journal of Geophysical Research, **102**, PP. 18,477–18,491.